PHYSICAL REVIEW C **76**, 054903 (2007)

Rapidity and species dependence of particle production at large transverse momentum for d+Au collisions at $\sqrt{s_{NN}} = 200$ GeV

B. I. Abelev,[50] J. Adams,[2] M. M. Aggarwal,[30] Z. Ahammed,[45] J. Amonett,[20] B. D. Anderson,[20] M. Anderson,[6] D. Arkhipkin,[13] G. S. Averichev,[12] Y. Bai,[28] J. Balewski,[17] O. Barannikova,[9] L. S. Barnby,[2] J. Baudot,[18] S. Bekele,[29] V. V. Belaga,[12] A. Bellingeri-Laurikainen,[40] R. Bellwied,[48] F. Benedosso,[28] S. Bhardwaj,[35] A. Bhasin,[19] A. K. Bhati,[30] H. Bichsel,[47] J. Bielcik,[50] J. Bielcikova,[50] L. C. Bland,[3] S.-L. Blyth,[22] B. E. Bonner,[36] M. Botje,[28] J. Bouchet,[40] A. V. Brandin,[26] A. Bravar,[3] M. Bystersky,[11] R. V. Cadman,[1] X. Z. Cai,[39] H. Caines,[50] M. Calderón de la Barca Sánchez,[6] J. Castillo,[28] O. Catu,[50] D. Cebra,[6] Z. Chajecki,[29] P. Chaloupka,[11] S. Chattopadhyay,[45] H. F. Chen,[38] J. H. Chen,[39] J. Cheng,[43] M. Cherney,[10] A. Chikanian,[50] W. Christie,[3] J. P. Coffin,[18] T. M. Cormier,[48] M. R. Cosentino,[37] J. G. Cramer,[47] H. J. Crawford,[5] D. Das,[45] S. Das,[45] M. Daugherity,[42] M. M. de Moura,[37] T. G. Dedovich,[12] M. DePhillips,[3] A. A. Derevschikov,[32] L. Didenko,[3] T. Dietel,[14] P. Djawotho,[17] S. M. Dogra,[19] W. J. Dong,[7] X. Dong,[38] J. E. Draper,[6] F. Du,[50] V. B. Dunin,[12] J. C. Dunlop,[3] M. R. Dutta Mazumdar,[45] V. Eckardt,[24] W. R. Edwards,[22] L. G. Efimov,[12] V. Emelianov,[26] J. Engelage,[5] G. Eppley,[36] B. Erazmus,[40] M. Estienne,[18] P. Fachini,[3] R. Fatemi,[23] J. Fedorisin,[12] K. Filimonov,[22] P. Filip,[13] E. Finch,[50] V. Fine,[3] Y. Fisyak,[3] J. Fu,[49] C. A. Gagliardi,[41] L. Gaillard,[2] M. S. Ganti,[45] V. Ghazikhanian,[7] P. Ghosh,[45] J. E. Gonzalez,[7] Y. G. Gorbunov,[10] H. Gos,[46] O. Grebenyuk,[28] D. Grosnick,[44] S. M. Guertin,[7] K. S. F. F. Guimaraes,[37] Y. Guo,[48] N. Gupta,[19] T. D. Gutierrez,[6] B. Haag,[6] T. J. Hallman,[3] A. Hamed,[48] J. W. Harris,[50] W. He,[17] M. Heinz,[50] T. W. Henry,[41] S. Hepplemann,[31] B. Hippolyte,[18] A. Hirsch,[33] E. Hjort,[22] A. M. Hoffman,[23] G. W. Hoffmann,[42] M. J. Horner,[22] H. Z. Huang,[7] S. L. Huang,[38] E. W. Hughes,[4] T. J. Humanic,[29] G. Igo,[7] P. Jacobs,[22] W. W. Jacobs,[17] P. Jakl,[11] F. Jia,[21] H. Jiang,[7] P. G. Jones,[2] E. G. Judd,[5] S. Kabana,[40] K. Kang,[43] J. Kapitan,[11] M. Kaplan,[8] D. Keane,[20] A. Kechechyan,[12] V. Yu. Khodyrev,[32] B. C. Kim,[34] J. Kiryluk,[23] A. Kisiel,[46] E. M. Kislov,[12] S. R. Klein,[22] A. Kocoloski,[23] D. D. Koetke,[44] T. Kollegger,[14] M. Kopytine,[20] L. Kotchenda,[26] V. Kouchpil,[11] K. L. Kowalik,[22] M. Kramer,[27] P. Kravtsov,[26] V. I. Kravtsov,[32] K. Krueger,[1] C. Kuhn,[18] A. I. Kulikov,[12] A. Kumar,[30] A. A. Kuznetsov,[12] M. A. C. Lamont,[50] J. M. Landgraf,[3] S. Lange,[14] S. LaPointe,[48] F. Laue,[3] J. Lauret,[3] A. Lebedev,[3] R. Lednicky,[13] C.-H. Lee,[34] S. Lehocka,[12] M. J. LeVine,[3] C. Li,[38] Q. Li,[48] Y. Li,[43] G. Lin,[50] X. Lin,[49] S. J. Lindenbaum,[27] M. A. Lisa,[29] F. Liu,[49] H. Liu,[38] J. Liu,[36] L. Liu,[49] Z. Liu,[49] T. Ljubicic,[3] W. J. Llope,[36] H. Long,[7] R. S. Longacre,[3] M. Lopez-Noriega,[29] W. A. Love,[3] Y. Lu,[49] T. Ludlam,[3] D. Lynn,[3] G. L. Ma,[39] J. G. Ma,[7] Y. G. Ma,[39] D. Magestro,[29] D. P. Mahapatra,[15] R. Majka,[50] L. K. Mangotra,[19] R. Manweiler,[44] S. Margetis,[20] C. Markert,[42] L. Martin,[40] H. S. Matis,[22] Yu. A. Matulenko,[32] C. J. McClain,[1] T. S. McShane,[10] Yu. Melnick,[32] A. Meschanin,[32] J. Millane,[23] M. L. Miller,[23] N. G. Minaev,[32] S. Mioduszewski,[41] C. Mironov,[20] A. Mischke,[28] D. K. Mishra,[15] J. Mitchell,[36] B. Mohanty,[22] L. Molnar,[33] C. F. Moore,[42] D. A. Morozov,[32] M. G. Munhoz,[37] B. K. Nandi,[16] C. Nattrass,[50] T. K. Nayak,[45] J. M. Nelson,[2] P. K. Netrakanti,[45] V. A. Nikitin,[13] L. V. Nogach,[32] S. B. Nurushev,[32] G. Odyniec,[22] A. Ogawa,[3] V. Okorokov,[26] M. Oldenburg,[22] D. Olson,[22] M. Pachr,[11] S. K. Pal,[45] Y. Panebratsev,[12] S. Y. Panitkin,[3] A. I. Pavlinov,[48] T. Pawlak,[46] T. Peitzmann,[28] V. Perevoztchikov,[3] C. Perkins,[5] W. Peryt,[46] V. A. Petrov,[48] S. C. Phatak,[15] R. Picha,[6] M. Planinic,[51] J. Pluta,[46] N. Poljak,[51] N. Porile,[33] J. Porter,[47] A. M. Poskanzer,[22] M. Potekhin,[3] E. Potrebenikova,[12] B. V. K. S. Potukuchi,[19] D. Prindle,[47] C. Pruneau,[48] J. Putschke,[22] G. Rakness,[31] R. Raniwala,[35] S. Raniwala,[35] R. L. Ray,[42] S. V. Razin,[12] J. Reinnarth,[40] D. Relyea,[4] F. Retiere,[22] A. Ridiger,[26] H. G. Ritter,[22] J. B. Roberts,[36] O. V. Rogachevskiy,[12] J. L. Romero,[6] A. Rose,[22] C. Roy,[40] L. Ruan,[22] M. J. Russcher,[28] R. Sahoo,[15] T. Sakuma,[23] S. Salur,[50] J. Sandweiss,[50] M. Sarsour,[41] P. S. Sazhin,[12] J. Schambach,[42] R. P. Scharenberg,[33] N. Schmitz,[24] K. Schweda,[22] J. Seger,[10] I. Selyuzhenkov,[48] P. Seyboth,[24] A. Shabetai,[22] E. Shahaliev,[12] M. Shao,[38] M. Sharma,[30] W. Q. Shen,[39] S. S. Shimanskiy,[12] E. Sichtermann,[22] F. Simon,[23] R. N. Singaraju,[45] N. Smirnov,[50] R. Snellings,[28] G. Sood,[44] P. Sorensen,[3] J. Sowinski,[17] J. Speltz,[18] H. M. Spinka,[1] B. Srivastava,[33] A. Stadnik,[12] T. D. S. Stanislaus,[44] R. Stock,[14] A. Stolpovsky,[48] M. Strikhanov,[26] B. Stringfellow,[33] A. A. P. Suaide,[37] E. Sugarbaker,[29] M. Sumbera,[11] Z. Sun,[21] B. Surrow,[23] M. Swanger,[10] T. J. M. Symons,[22] A. Szanto de Toledo,[37] A. Tai,[7] J. Takahashi,[37] A. H. Tang,[3] T. Tarnowsky,[33] D. Thein,[7] J. H. Thomas,[22] A. R. Timmins,[2] S. Timoshenko,[26] M. Tokarev,[12] T. A. Trainor,[47] S. Trentalange,[7] R. E. Tribble,[41] O. D. Tsai,[7] J. Ulery,[33] T. Ullrich,[3] D. G. Underwood,[1] G. Van Buren,[3] N. van der Kolk,[28] M. van Leeuwen,[22] A. M. Vander Molen,[25] R. Varma,[16] I. M. Vasilevski,[13] A. N. Vasiliev,[32] R. Vernet,[18] S. E. Vigdor,[17] Y. P. Viyogi,[15] S. Vokal,[12] S. A. Voloshin,[48] W. T. Waggoner,[10] F. Wang,[33] G. Wang,[7] J. S. Wang,[21] X. L. Wang,[38] Y. Wang,[43] J. W. Watson,[20] J. C. Webb,[44] G. D. Westfall,[25] A. Wetzler,[22] C. Whitten Jr.,[7] H. Wieman,[22] S. W. Wissink,[17] R. Witt,[50] J. Wood,[7] J. Wu,[38] N. Xu,[22] Q. H. Xu,[22] Z. Xu,[3] P. Yepes,[36] I.-K. Yoo,[34] V. I. Yurevich,[12] W. Zhan,[21] H. Zhang,[3] W. M. Zhang,[20] Y. Zhang,[38] Z. P. Zhang,[38] Y. Zhao,[38] C. Zhong,[39] R. Zoulkarneev,[13] Y. Zoulkarneeva,[13] A. N. Zubarev,[12] and J. X. Zuo[39]

(STAR Collaboration)

[1]*Argonne National Laboratory, Argonne, Illinois 60439, USA*

[2]*University of Birmingham, Birmingham, United Kingdom*

[3]*Brookhaven National Laboratory, Upton, New York 11973, USA*

[4]*California Institute of Technology, Pasadena, California 91125, USA*

[5]*University of California, Berkeley, California 94720, USA*

[6]*University of California, Davis, California 95616, USA*

[7]*University of California, Los Angeles, California 90095, USA*

[8]*Carnegie Mellon University, Pittsburgh, Pennsylvania 15213, USA*

[9]*University of Illinois, Chicago, USA*
[10]*Creighton University, Omaha, Nebraska 68178, USA*
[11]*Nuclear Physics Institute AS CR, 250 68 Řež/Prague, Czech Republic*
[12]*Laboratory for High Energy (JINR), Dubna, Russia*
[13]*Particle Physics Laboratory (JINR), Dubna, Russia*
[14]*University of Frankfurt, Frankfurt, Germany*
[15]*Institute of Physics, Bhubaneswar 751 005, India*
[16]*Indian Institute of Technology, Mumbai, India*
[17]*Indiana University, Bloomington, Indiana 47408, USA*
[18]*Institut de Recherches Subatomiques, Strasbourg, France*
[19]*University of Jammu, Jammu 180 001, India*
[20]*Kent State University, Kent, Ohio 44242, USA*
[21]*Institute of Modern Physics, Lanzhou, People's Republic of China*
[22]*Lawrence Berkeley National Laboratory, Berkeley, California 94720, USA*
[23]*Massachusetts Institute of Technology, Cambridge, Massachusetts 02139-4307, USA*
[24]*Max-Planck-Institut für Physik, Munich, Germany*
[25]*Michigan State University, East Lansing, Michigan 48824, USA*
[26]*Moscow Engineering Physics Institute, Moscow Russia*
[27]*City College of New York, New York City, New York 10031, USA*
[28]*NIKHEF and Utrecht University, Amsterdam, The Netherlands*
[29]*Ohio State University, Columbus, Ohio 43210, USA*
[30]*Panjab University, Chandigarh 160 014, India*
[31]*Pennsylvania State University, University Park, Pennsylvania 16802, USA*
[32]*Institute of High Energy Physics, Protvino, Russia*
[33]*Purdue University, West Lafayette, Indiana 47907, USA*
[34]*Pusan National University, Pusan, Republic of Korea*
[35]*University of Rajasthan, Jaipur 302 004, India*
[36]*Rice University, Houston, Texas 77251, USA*
[37]*Universidade de Sao Paulo, Sao Paulo, Brazil*
[38]*University of Science & Technology of China, Hefei 230026, People's Republic of China*
[39]*Shanghai Institute of Applied Physics, Shanghai 201800, People's Republic of China*
[40]*SUBATECH, Nantes, France*
[41]*Texas A&M University, College Station, Texas 77843, USA*
[42]*University of Texas, Austin, Texas 78712, USA*
[43]*Tsinghua University, Beijing 100084, People's Republic of China*
[44]*Valparaiso University, Valparaiso, Indiana 46383, USA*
[45]*Variable Energy Cyclotron Centre, Kolkata 700 064, India*
[46]*Warsaw University of Technology, Warsaw, Poland*
[47]*University of Washington, Seattle, Washington 98195, USA*
[48]*Wayne State University, Detroit, Michigan 48201, USA*
[49]*Institute of Particle Physics, CCNU (HZNU), Wuhan 430079, People's Republic of China*
[50]*Yale University, New Haven, Connecticut 06520, USA*
[51]*University of Zagreb, Zagreb, HR-10002, Croatia*

(Received 14 September 2006; published 5 November 2007)

We determine rapidity asymmetry in the production of charged pions, protons, and antiprotons for large transverse momentum (p_T) for d+Au collisions at $\sqrt{s_{NN}} = 200$ GeV. The rapidity asymmetry is defined as the ratio of particle yields at backward rapidity (Au beam direction) to those at forward rapidity (d beam direction). The identified hadrons are measured in the rapidity regions $|y| < 0.5$ and $0.5 < |y| < 1.0$ for the p_T range $2.5 < p_T < 10\,\mathrm{GeV/c}$. We observe significant rapidity asymmetry for charged pion and proton+antiproton production in both the rapidity regions. The asymmetry is larger for $0.5 < |y| < 1.0$ than for $|y| < 0.5$ and is almost independent of particle type. The measurements are compared to various model predictions employing multiple scattering, energy loss, nuclear shadowing, saturation effects, and recombination and also to a phenomenological parton model. We find that asymmetries are sensitive to model parameters and show model preference. The rapidity dependence of π^-/π^+ and $\bar{p}/p$ ratios in peripheral d+Au and forward neutron-tagged events are used to study the contributions of valence quarks and gluons to particle production at high p_T.

DOI: 10.1103/PhysRevC.76.054903 PACS number(s): 25.75.Dw, 13.85.−t

I. INTRODUCTION

The mechanisms for particle production in d+Au collisions at the Relavtistic Heavy Ion Collider (RHIC) may be different at forward and backward rapidities. The partons from the deuteron-side (forward rapidity) are expected to undergo multiple scattering while traversing the gold nucleus. Those on the gold side (backward rapidity) are likely to be affected by the properties of the nucleus. A comparative study of particle production at forward and backward rapidity can be carried out using a ratio called the rapidity asymmetry ($Y_{\rm Asym}$), which is defined as

$$Y_{\rm Asym}(p_T) = \frac{Y_B(p_T)}{Y_F(p_T)},$$

where Y_F and Y_B are forward and backward particle yields, respectively. $Y_{\rm Asym}$ may provide unique information to help determine the relative contributions of various physics processes to particle production, such as multiple scattering, nuclear shadowing, recombination of thermal partons, and parton saturation.

Recently, models incorporating different physics effects have described the nuclear modification factor for d+Au collisions ($R_{\rm dAu}$). Models including shadowing effects or nuclear modifications to the nucleon parton distributions reproduce reasonably well $R_{\rm dAu}$ for inclusive charged hadrons [1]. Those based on transverse-momentum broadening (Cronin effect [2]), dynamical shadowing, and energy loss in cold nuclear matter [3] also give $R_{\rm dAu}$ predictions for inclusive charged hadrons, consistent with the experimental data. Models based on the color glass condensate (CGC) approach reproduce the p_T dependence of inclusive charged hadron $R_{\rm dAu}$ at both mid- and forward rapidity [4]. These models also qualitatively describe the pseudorapidity asymmetry for inclusive charged hadrons in d+Au collisions [5].

Another approach based on hadronization by recombination of thermal partons at lower $p_{\rm T}$ has been quite successful in describing the observed $R_{\rm dAu}$ for charged hadrons at RHIC [6]. This approach emphasizes the hadronization portion of the final-state interaction. Although it takes into account the hard scattering in pQCD, the fragmentation is replaced by recombination of soft and shower partons in the intermediate p_T region. Also, a phenomenological approach called EPOS [7], based on a parton model, has described the d+Au collision data at RHIC. In this model the nuclear effects are included through elastic and inelastic parton ladder splitting.

It is of interest to see how these models compare to data for rapidity asymmetry of identified hadrons from d+Au collisions. More precisely, identified hadron $Y_{\rm Asym}$, a more differential quantity, may allow some determination of the relative contribution of the physical processes discussed above. Strong particle type (baryon and meson) dependence of the nuclear modification factor and azimuthal anisotropy at intermediate $p_{\rm T}(2 < p_T < 6\,{\rm GeV}/c)$ has been observed in Au+Au collisions at RHIC [8]. The present study will investigate if such particle type (baryon and meson) dependence is observed in $Y_{\rm Asym}$ for d+Au collisions.

In addition to providing insight into different particle production mechanisms at forward and backward rapidity for d+Au collisions, the measurements presented here may be used to study the presence of possible effects of valence quarks and isospin on particle production. At high p_T and rapidities away from midrapidity, the role of valence quarks becomes increasingly dominant. Such studies are even more interesting for n-tag events (events where the neutron in the deuteron does not interact with the gold nucleus). A comparative study between p+Au (n-tag) and d+Au data is of interest. For n-tag events at forward rapidity and high p_T, the two valence u quarks in the proton of the deuteron should lead to more production of π^+ ($u\bar{d}$) compared to π^- ($d\bar{u}$). For backward rapidities, if the flavor distribution in sea quarks is uniform and the incoming gold nucleus has no asymmetry in u and d quarks, one expects the ratio $\pi^-/\pi^+ \sim 1$. This difference between forward and backward rapidity may be more pronounced for $\bar{p}/p$. Study of particle ratios as a function of rapidity at high p_T in peripheral and n-tag events for d+Au collisions may provide some information on the flavor dependence of particle production. These ratios are in principle sensitive to the fragmentation function ratios of u quarks to π^- and π^+ [9], to the ratio of (u, d) quarks fragmenting to protons [10], and to the fractional contributions of quarks and gluons to hadrons at a given momentum.

In this article, we present the first results for the rapidity asymmetry of charged pion, proton, and antiproton production at high p_T for d+Au collisions at $\sqrt{s_{NN}} = 200$ GeV measured by the STAR experiment [11] at RHIC. A similar study for inclusive charged hadrons has been reported in Ref. [5]. The asymmetry is studied as a function of p_T for different collision centralities in the two rapidity regions $|y| < 0.5$ and $0.5 < |y| < 1.0$. The beam rapidity in such collisions is at $\eta \sim 5.36$. In Sec. II we discuss the detectors used in the analysis, trigger and centrality selection, particle identification at high p_T, and the systematic errors. In Sec. III we discuss the rapidity, p_T, species, and centrality dependence of $Y_{\rm Asym}$. In Sec. IV, the $Y_{\rm Asym}$ results are compared to calculations from various models discussed earlier. In Sec. V, we present the rapidity dependence of the nuclear modification factor for $\pi^+ + \pi^-$ and $p + \bar{p}$. In Sec. VI, we study the antiparticle to particle ratios as a function of rapidity at high $p_{\rm T}$ in n-tag and peripheral d+Au events to investigate the flavor dependence of particle production. Section VII completes this work with the summary of our findings.

II. EXPERIMENT AND ANALYSIS

A. Detectors

For the present analysis we use data recorded by the Time Projection Chamber (TPC) [12] in the STAR experiment at RHIC. The TPC is STAR's primary tracking device. It is 4.2 m long and 4 m in diameter. The sensitive volume of the TPC contains P10 gas (10% methane, 90% argon) regulated at 2 mbar above atmospheric pressure. The TPC data are used to determine particle trajectories, momenta, and particle-type through ionization energy loss (dE/dx). Its acceptance covers ± 1.8 units of pseudorapidity (η) and the full azimuthal angle. Charged particle momenta are determined from the TPC data for the d+Au run in the year 2003 in which STAR's solenoidal

magnet field was set to 0.5 T. Two zero degree calorimeters (ZDCs) [13] situated along both sides of the beam axis, about 18 m from the nominal collision point (center of TPC), were used for triggering. The collision centrality is obtained from the charged hadron multiplicity measured by STAR's Forward Time Projection Chambers (FTPCs) [14]. The details of the design and other characteristics of the detectors can be found in Ref. [11]. The details of the trigger condition, collision centrality selection, and method of high p_T particle identification are described below.

B. Trigger conditions

The ZDC in the Au beam direction, which is assigned negative pseudorapidity (η), was used as the trigger detector for obtaining the minimum bias data. The minimum bias trigger required a ZDC signal equal to or larger than that expected from a single neutron. The trigger efficiency was found to be $95 \pm 3\%$ of the d+Au hadronic cross section $\sigma_{\rm hadr}^{d\rm Au}$. Trigger related backgrounds were determined using data recorded for beam crossings without collisions. For the n-tag events, the ZDC in the deuteron beam direction was used. Such events were required to have at least one beam rapidity neutron in the ZDC. The cross section for such a process was measured to be $(19.2 \pm 1.3)\%$ of $\sigma_{\rm hadr}^{d\rm Au}$. The vertex was reconstructed for $93 \pm 1\%$ of triggered minimum bias events. A total of 11.7 million minimum bias d+Au events and 2.0 million n-tag events having a vertex within ± 30 cm of the nominal interaction point along the beam direction were analyzed. Two rapidity regions were used: $|y| < 0.5$ and $0.5 < |y| < 1.0$, and the p_T range was $2.5 < p_T < 10\,{\rm GeV}/c$. The p_T spectra were corrected for trigger and vertex-finding inefficiencies. In the present work the trigger conditions for obtaining the minimum bias data are similar to as discussed in Ref. [15].

C. Collision centrality

Uncorrected charged track multiplicity ($N_{\rm chtrk}^{\rm FTPC}$) measured within $-3.8 < \eta < -2.8$ by the FTPC was used to determine the collision centrality for d+Au collisions. Figure 1 shows the charged track multiplicity in FTPC in the Au beam direction for minimum bias d+Au collisions and ZDC neutron-tagged events. The latter have a strong bias toward low multiplicity. The FTPC in the Au beam direction and the ZDC in d beam direction are separated by eight units in rapidity. The centrality selection criteria is given in Table I, along with the average number of binary collisions ($N_{\rm bin}$) and the number of participating nucleons ($N_{\rm part}$) estimated using a Monte Carlo Glauber calculation [16] incorporating the Hulthén wave function of the deuteron [17]. In this model $\sigma_{\rm hadr}^{d\rm Au} = 2.21 \pm 0.09$b, and $N_{\rm bin}$ for n-tag events is 2.9 ± 0.2. The FTPC (Au beam direction) multiplicity distribution was modeled by convoluting the Glauber model distribution of participants from the Au nucleus with the charged multiplicity distribution measured in $2.5 < |\eta| < 3.5$ for $\bar{p} + p$ collisions at $\sqrt{s} = 200$ GeV [18]. The FTPC acceptance, efficiency, and backgrounds were taken into account using HIJING [19] events in a GEANT model of the detector. This model provides reasonable agreement with the measured charged track multiplicity distribution in the FTPC and the single neutron cross section measured by the ZDC on the deuteron side (Fig. 1). In Fig. 1 we also show the cut defining the 20% highest multiplicity collisions in the d+Au data. Further details of centrality tagging in d+Au collisions can be found in Ref. [15].

TABLE I. Centrality selection, number of participating nucleons, and number of binary collisions for d+Au collisions at $\sqrt{s_{NN}} = 200$ GeV.

% cross section	$N_{\rm chtrk}^{\rm FTPC}$	$\langle N_{\rm part} \rangle$	$\langle N_{\rm bin} \rangle$
0–20	> 17	15.67 ± 1.07	15.1 ± 1.15
20–40	11–17	11.16 ± 1.25	10.6 ± 1.38
40–100	< 11	5.14 ± 0.47	4.2 ± 0.51
0–100	> 0	8.31 ± 0.34	7.5 ± 0.38

D. Particle identification at high p_T

Particle identification at high transverse momenta ($p_{\rm T} > 2.5\,{\rm GeV}/c$) is done by exploiting the relativistic rise of the ionization energy loss. Here we briefly describe the identification procedure (see Ref. [20,21]). For $2.5 < p_T \lesssim 10\,{\rm GeV}/c$, there is a difference of about 10–20% between the pion dE/dx and the dE/dx for kaons and protons, due to the relativistic rise of the ionization energy loss for pions. This results in a few sigma (1–3σ) separation. The dE/dx resolution is $\sim$8% [20].

Pions are the dominant component of the hadron yield for d+Au collisions at RHIC. The prominent peak in the dE/dx distribution is used to determine the pion yield in this p_T range. To extract the pion yield in a given p_T bin, we performed a six Gaussian fit to the normalized dE/dx distributions of positive and negative hadrons simultaneously. The normalized dE/dx in general is defined as $n\sigma_X = \log[(dE/dx)/B_X]/\sigma_X$,

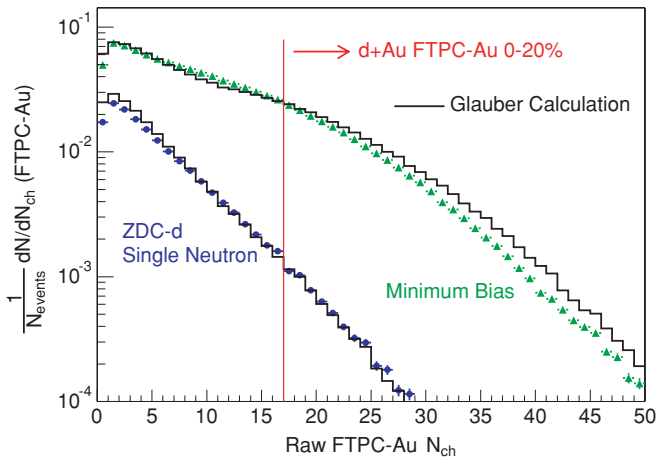

FIG. 1. (Color online) Uncorrected charged particle multiplicity distributions measured in $-3.8 < \eta < -2.8$ (Au direction) for d+Au collisions. Points are for minimum bias (triangles) and peripheral (circles, ZDC-d single neutron) collisions [15]. Both are normalized to the total number of d+Au collisions. Histograms are Glauber model calculations.

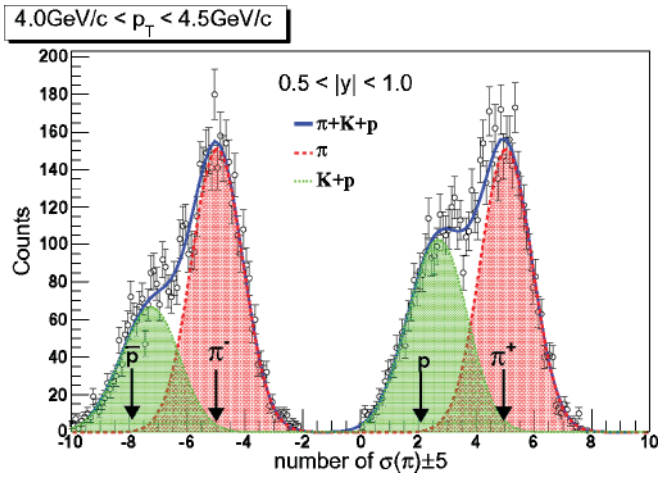

FIG. 2. (Color online) dE/dx distribution normalized by pion dE/dx at $4.0 < p_T < 4.5\,\mathrm{GeV}/c$ and $0.5 < |\eta| < 1.0$, shifted by ± 5 for positive and negative charged particles, respectively. The distributions are for minimum bias d+Au collisions. The pion, proton, and antiproton peak positions are indicated by arrows.

where X can be $e^{\pm}, \pi^{\pm}, K^{\pm}$, or $p(\bar{p})$. B_X is the expected mean dE/dx of particle X, and σ_X is the dE/dx resolution of the TPC and is a function of the track length in TPC. The expected mean dE/dx of particle X is calculated using Bichsel function for the energy loss in thin layers of P10 for STAR TPC [12,22]. The good agreement between the measurement and the calculation can be found in Ref. [20].

Figure 2 shows a typical dE/dx distribution normalized to pion dE/dx (referred to as the $n\sigma_\pi$ distribution) for charged hadrons with $4.0 < p_T < 4.5\,\mathrm{GeV}/c$ and $0.5 < |\eta| < 1.0$. For clarity of presentation, the $n\sigma_\pi$ distributions in Fig. 2 are shifted by ± 5 for positively and negatively charged particles, respectively. The $n\sigma_\pi$ distribution is a normal Gaussian distribution for an ideal calibration. The six Gaussians are for $\pi^{\pm}$, $K^{\pm}$, and $p(\bar{p})$. The relative peak positions of the kaons and protons with respect to pion peak position in the $n\sigma_\pi$ distribution are estimated by studying the difference between dE/dx distribution normalized to pion dE/dx and dE/dx distribution normalized to kaon dE/dx, dE/dx distribution normalized to proton dE/dx and the dE/dx distribution normalized to pion dE/dx for positively and negatively charged particles. The widths of the six Gaussians are taken to be the same. The Gaussian distribution used to extract the pion yield and the pion, proton, and antiproton peak positions are also shown in the figure.

The proton yield is obtained by integrating the entries (Y) in the low part of the dE/dx distribution, about 2.5σ away from the pion dE/dx peak. The integration limits were varied to check the stability of the results. The yield Y can be expressed as

$$Y = \alpha p + \beta K,$$

where α and β are the proton and kaon efficiencies (fraction of the respective Gaussians inside the integration region) from the integration described above, derived from the dE/dx calibration, resolution, and the Bichsel function [20,22]. The kaon contamination to the proton yield is estimated by using two independent procedures. In the first case the kaon contamination is estimated through the yields of the inclusive hadrons (h) and pions (π); in the second case using K^0_S measurements [21] (only available for $|y| < 0.5$ up to $p_T < 5\,\mathrm{GeV}/c$). The raw proton yield is then obtained as

$$p = [Y - \beta(h - \pi)]/(\alpha - \beta)$$

or

$$p = \left(Y - \beta K^0_S\right)/\alpha.$$

The typical values of α for a dE/dx cut slightly away from the proton peak position is 0.4. The β values decrease from 0.2 to 0.08 with p_T in the range $2.5 < p_T < 10\,\mathrm{GeV}/c$. At high p_T, the yields of other stable particles (i.e., electrons and deuterons) are at least two orders of magnitude smaller than those of pions and are negligible for our studies. The two results are consistent in the region where STAR K^0_S measurements are available. Because the energy loss of particles in the TPC is almost independent of charge sign, the dependence of h^-/h^+ on $n\sigma_\pi$ is due to different particle composition and the dE/dx separation between pions, kaons, and protons [20]. This can provide a consistency check for the yields.

The dE/dx resolution is better for longer tracks, shorter drift distance, stronger magnetic field, smaller multiplicity, and lower beam luminosity. Due to longer tracks and shorter drift distances for particles produced at higher Y, the dE/dx resolution gets better. Thus, the separations between pions and kaons or (anti-)protons were larger for $0.5 < |y| < 1.0$ than for $|y| < 0.5$ [21], and particle identification is easier at larger p_T.

E. Correction factors

The various correction factors for the identified hadron spectra are listed in Table II. The trigger and vertex efficiencies were discussed previously. The identified hadron track reconstruction efficiency was estimated by embedding Monte Carlo particles into the real data and then following the full reconstruction procedure. It was observed to be independent of p_T for $p_T > 2.5\,\mathrm{GeV}/c$ for both rapidity regions. The reconstruction efficiency for $p_T > 2.5\,\mathrm{GeV}/c$ for charged pions and protons are ~92 and ~90%, respectively, in the rapidity region $|y| < 0.5$. For $0.5 < |y| < 1.0$, the

TABLE II. Correction factors for identified hadron spectra at high p_T ($> 2.5\,\mathrm{GeV}/c$) for minimum bias d+Au collisions.

Type	%
Trigger efficiency	95 ± 3
Vertex efficiency	93 ± 1
Track reconstruction efficiency ($\|y\| < 0.5$)	$\sim 90 \pm 8$
Track reconstruction efficiency ($0.5 < \|y\| < 1.0$)	$\sim 82 \pm 8$
Background contamination	$\sim 5 \pm 1$

TABLE III. Systematic errors for identified hadron minimum bias yields at high p_T ($> 2.5\,\mathrm{GeV}/c$) for d+Au collisions.

Sources of uncertainty	% Error
Modeling detector response	8
Momentum resolution	4 (at $p_T = 7\,\mathrm{GeV}/c$)
Spatial distortion	8
dE/dx pion peak position	8
dE/dx proton peak position	8
Kaon contamination to proton yield	12 (at $p_T = 7\,\mathrm{GeV}/c$)
Protons from hyperon decay	7 (at $p_T = 7\,\mathrm{GeV}/c$)
Normalization (trigger and luminosity)	10

reconstruction efficiency for charged pions and protons is ~82 and 84%, respectively. The background contamination in the pion spectra for $p_T > 2.5\,\mathrm{GeV}/c$, primarily from K^S_0 weak decay, is ~5%. No strong centrality dependence was observed in the correction factors. The charged pion, proton, and antiproton spectra are corrected for efficiency and background effects. The inclusive proton and antiproton spectra are presented without hyperon feed down corrections [21,23]. Preliminary study shows that the ratio of Λ to inclusive p in the rapidity range $|y| < 0.5$ decreases from 0.7 to 0.3 with increase in p_T from 2.5 to 5.5 GeV/c. For the p_T range studied, the effect of absorption of $\bar{p}$ in the detector material is less than 1% [24].

F. Systematic errors

The total systematic uncertainties associated with the pion yields are estimated to be $\lesssim 15\%$, and those for proton and antiproton yields are estimated to be $\lesssim 22\%$. They are of similar order for both the rapidity regions, and the average values for minimum bias collisions are given in Table III.

The sources of systematic error on the high p_T yield arise owing to (a) uncertainty in modeling the detector response in the Monte Carlo simulations, (b) momentum resolution (increases with p_T) [21], (c) difference in the yields for different TPC sectors as a result of spatial distortion effects, (d) uncertainty in determining the pion and proton dE/dx peak positions, (e) uncertainty in estimating the kaon contamination to proton yields (increases from 7% at $p_T = 2.5\,\mathrm{GeV}/c$ to 15% at $p_T = 10\,\mathrm{GeV}/c$), and (f) uncertainty due to protons from hyperon decay that are reconstructed as primordial protons at a slightly higher p_T than their true value, with a worse momentum resolution (increases from 2% at $p_T = 2.5\,\mathrm{GeV}/c$ to 10% at $p_T = 10\,\mathrm{GeV}/c$). There is an additional 10% [15] normalization uncertainty due to trigger and luminosity uncertainties. These systematic errors are not shown in Figure 3.

As this work focuses mainly on ratios such as Y_{Asym}, most of the systematic errors cancel. The resultant systematic error on Y_{Asym} is about 5%. The errors shown for figures with ratios are statistical and systematic errors added in quadrature.

Figure 3 shows the measured invariant yields of charged pions, protons, and antiprotons for the p_T range $2.5 < p_T < 10\,\mathrm{GeV}/c$ in the rapidity regions $|y| < 0.5$ (solid symbols) and $0.5 < |y| < 1.0$ (open symbols) for minimum bias and various collision centrality classes for d+Au collisions at $\sqrt{s_{NN}} = 200\,\mathrm{GeV}$. The p_T spectra are corrected for the trigger, vertex, and reconstruction efficiencies and the background effects listed in Table II. The p_T bin width used in the analysis are 0.5 GeV/c for $p_T > 5\,\mathrm{GeV}/c$ and 1.0 GeV/c for $p_T > 5\,\mathrm{GeV}/c$.

III. RAPIDITY ASYMMETRY

In this section we discuss the y, p_T, species and centrality dependence of Y_{Asym}.

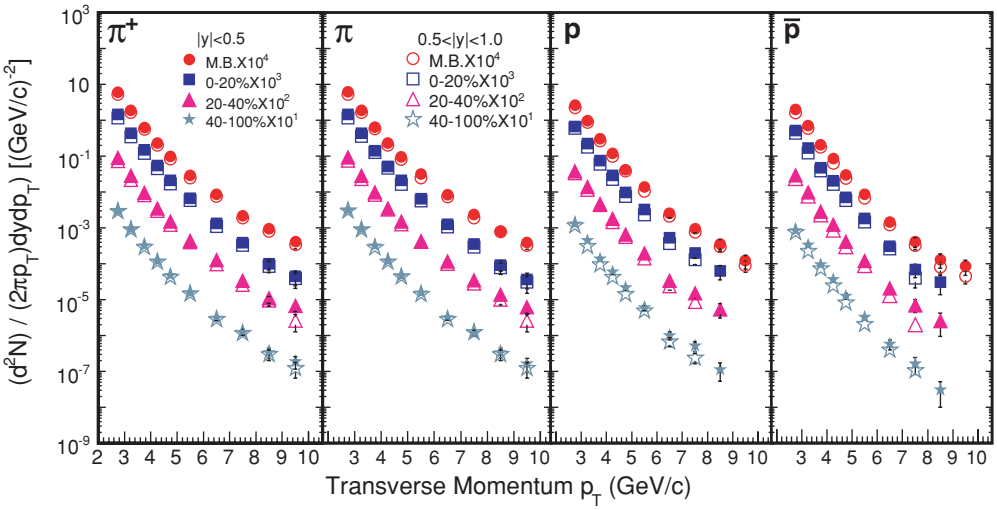

FIG. 3. (Color online) High transverse-momentum spectra ($p_T > 2.5\,\mathrm{GeV}/c$) of charged pions, protons, and antiprotons for the rapidity regions $|y| < 0.5$ (solid symbols) and $0.5 < |y| < 1.0$ (open symbols) for d+Au collisions and various event centrality classes at $\sqrt{s_{NN}} =$ 20 GeV.

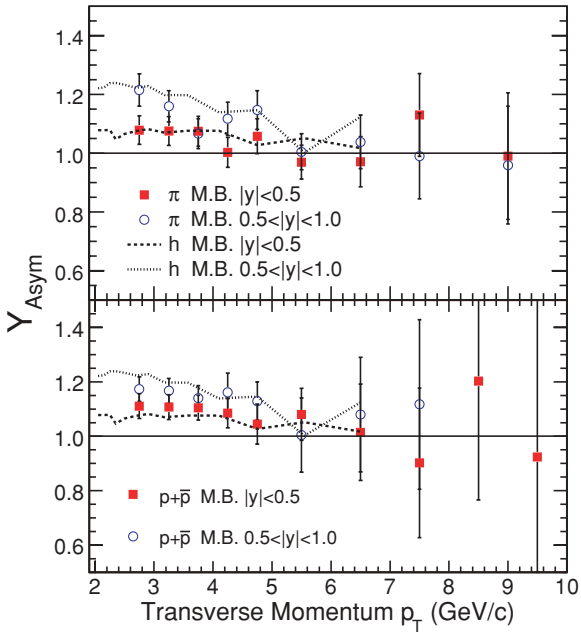

FIG. 4. (Color online) High transverse-momentum rapidity asymmetry factor ($Y_{\rm Asym}$) for $\pi^+ + \pi^-$ and $p + \bar{p}$ for $|y| < 0.5$ and $0.5 < |y| < 1.0$ for minimum bias d+Au collisions at $\sqrt{s_{NN}} =$ 200 GeV. For comparison the inclusive charged hadron results from STAR [5] are also shown by the curves.

A. Rapidity, transverse momentum, and species dependence

Figure 4 shows the high p_T dependence of $Y_{\rm Asym}$ for $\pi^+ + \pi^-$ and $p + \bar{p}$ for the rapidity regions $|y| < 0.5$ and $0.5 < |y| < 1.0$ for minimum bias events. The backward rapidity is considered as the gold-side and corresponds to the negative rapidity region. The forward rapidity is the deuteron side and corresponds to positive rapidity. For comparison the pseudorapidity asymmetry for charged hadrons [5] is shown also in the figure. The following observations are made:

(i) $Y_{\rm Asym}$ is found to be larger for $0.5 < |y| < 1.0$ than for $|y| < 0.5$ for all the hadrons with $2.5 > p_T > 5\,{\rm GeV}/c$. This may indicate the presence of some rapidity dependence of nuclear effects such as parton saturation, nuclear shadowing, or energy loss in cold nuclear matter.

(ii) The $Y_{\rm Asym}$ values are consistent with unity for both rapidity regions at high $p_T (> 5.5\,{\rm GeV}/c)$, suggesting absence of nuclear effects on particle production in d+Au collisions for this p_T range. A straight line fit to the $Y_{\rm Asym}(\pi)$ values for $p_T (> 5.5\,{\rm GeV}/c$ gives 0.99 ± 0.04 and 1.01 ± 0.04 for $|y| < 0.5$ and $0.5 < |y| < 1.0$, respectively.

(iii) $Y_{\rm Asym}$ for charged pions is greater than unity and seems to decrease with increasing p_T for $2.5 < p_T < 5\,{\rm GeV}/c$. Although $Y_{\rm Asym}$ for $p + \bar{p}$ is also greater than unity, the trend seems to be toward a constant value in this p_T range. These features are opposite to predictions from a model based on incoherent initial multiple partonic scattering and independent fragmentation [25], like HIJING [19]. Such a model predicts that $Y_{\rm Asym}$ is less than unity at intermediate p_T and approximately unity for larger p_T [5].

(iv) For $|y| < 0.5$, $Y_{\rm Asym}$ for $p + \bar{p}$ is slightly larger than it is for charged pions for $2.5 < p_T < 4\,{\rm GeV}/c$. For $0.5 < |y| < 1.0$ no strong particle type dependence is observed for $Y_{\rm Asym}$. This is in contrast to the observed baryon-meson differences for the same p_T range for Au+Au collisions, which were described by recombination-based models [26].

The rapidity asymmetries in particle production at low p_T are consistent with those seen in the total $dN_{\rm ch}/d\eta$ [27,28].

B. Centrality dependence

In Fig. 5 we show the centrality dependence of $Y_{\rm Asym}$ at high p_T for $\pi^+ + \pi^-$ and $p + \bar{p}$ for the two rapidity regions $|y| < 0.5$ (left panels) and $0.5 < |y| < 1.0$ (right panels). The data are shown only for $2.5 < p_T > 5.5\,{\rm GeV}/c$. The $Y_{\rm Asym}$ values approach unity for the centrality classes studied for $p_T (> 5.5\,{\rm GeV}/c$ in both the rapidity regions. For $|y| < 0.5$, a prominent centrality dependence of $Y_{\rm Asym}$ is not observed. For $0.5 < |y| < 1.0$, $Y_{\rm Asym}$ is larger for central (0–20%) compared to peripheral (40–100%) events for $2.5 < p_T < 4\,{\rm GeV}/c$. The indication of a centrality dependence in the $Y_{\rm Asym}$ at $0.5 < |y| < 1.0$ is consistent with predictions from saturation models [4]. However, in such models the centrality dependence is much stronger than observed in the present data [5].

IV. MODEL COMPARISON

In this section we compare the measured high p_T identified hadron $Y_{\rm Asym}$ in the rapidity regions $|y| < 0.5$ and $0.5 < |y| < 1.0$ for minimum bias d+Au collisions at $\sqrt{s_{NN}} = 200\,{\rm GeV}$ with predictions from various models (Figs. 6–10).

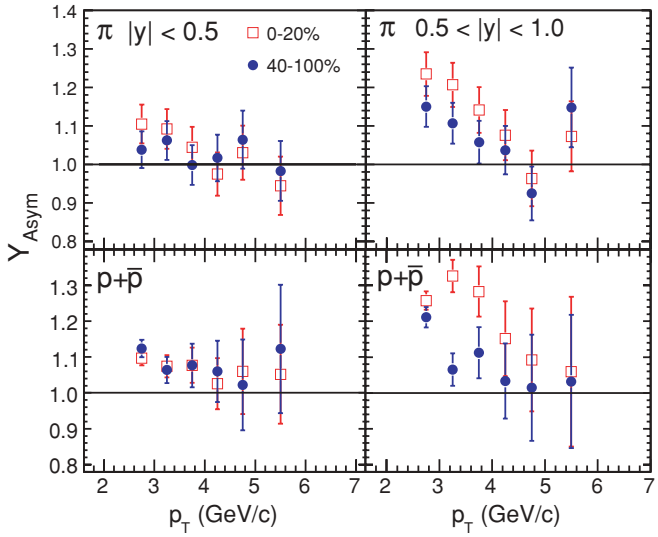

FIG. 5. (Color online) Centrality dependence of high transverse-momentum rapidity asymmetry factor ($Y_{\rm Asym}$) for $\pi^+ + \pi^-$ and $p + \bar{p}$ at $|y| < 0.5$ (left panels) and $0.5 < |y| < 1.0$ (right panels) for d+Au collisions at $\sqrt{s_{NN}} = 200$ GeV.

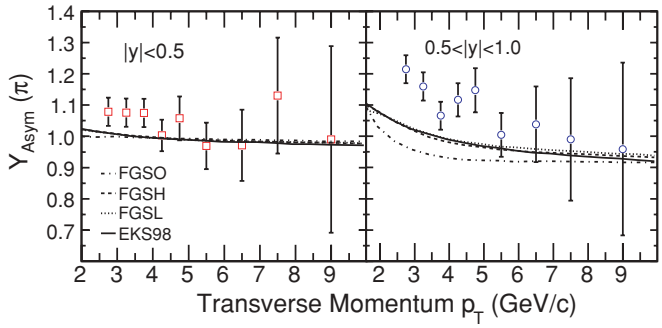

FIG. 6. (Color online) High transverse-momentum rapidity asymmetry factor ($Y_{\rm Asym}$) for $\pi^+ + \pi^-$ at $|y| < 0.5$ and $0.5 < |y| < 1.0$ for minimum bias d+Au collisions at $\sqrt{s_{NN}} = 200$ GeV compared to a model with only nuclear shadowing [1]. The different curves represent different parametrization of nuclear shadowing. See text for more details.

A. Comparison to the nuclear shadowing model

First we compare the high p_T charged pion $Y_{\rm Asym}$ in both rapidity regions with model predictions that incorporate only nuclear shadowing [1]. In these calculations two parametrizations of nuclear shadowing, covering the extremes of gluon shadowing at low x, are taken. The parametrization by Eskola *et al.* [29] is referred to as EKS98. The other, FGS, is from Frankfurt, Guzey, and Strikman [30] (FGSO, the original parametrization, along with FGSH and FGSL for high and low gluon shadowing). The calculations use MRST leading order (LO) parton distribution functions [31]. The fragmentation of produced partons into charged pions uses the LO Kniehl-Kramer-Potter (KKP) fragmentation functions [32] obtained from a fit to $e^+ + e^-$ data. In EKS98 the valence quark shadowing is identical for u and d quarks at the minimum momentum scale of the hard interaction. In FGS the EKS98 valence quark shadowing ratios are used as input, along with Gribov theory and hard diffraction. The charged hadron $R_{\rm dAu}$ was reasonably well described by such a model using the FGS parametrization [1].

Our charged pion data (Fig. 6) indicate that nuclear shadowing as implemented in the models discussed cannot explain the measured $Y_{\rm Asym}$ for $2.5 < p_T < 5\,{\rm GeV}/c$ for both $|y| < 0.5$ and $0.5 < |y| < 1.0$. The differences between data and model increase with increasing rapidity. At larger p_T, the data values approach unity, indicating an absence of nuclear effects. The effect on $Y_{\rm Asym}$ of using a different parametrization of nuclear shadowing at high p_T is found to be negligible for $|y| < 0.5$. However, some differences are observed in FGS for $0.5 < |y| < 1.0$.

$Y_{\rm Asym}$ from the nuclear shadowing model covering the extremes of gluon shadowing at low x is not consistent with the measured values. The comparison therefore provides an idea of the maximum contribution to $Y_{\rm Asym}$ from only nuclear shadowing in d+Au collisions at $\sqrt{s_{NN}} = 200$ GeV.

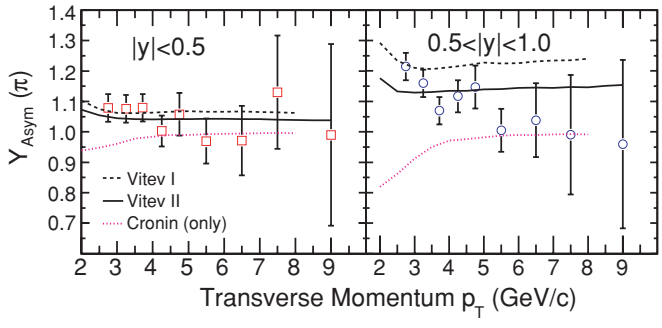

FIG. 7. (Color online) High transverse-momentum rapidity asymmetry factor ($Y_{\rm Asym}$) for $\pi^+ + \pi^-$ at $|y| < 0.5$ and $0.5 < |y| < 1.0$ for minimum bias d+Au collisions at $\sqrt{s_{NN}} = 200$ GeV compared to models incorporating multiple scattering, shadowing, and energy loss in cold nuclear matter [3]. See text for more details.

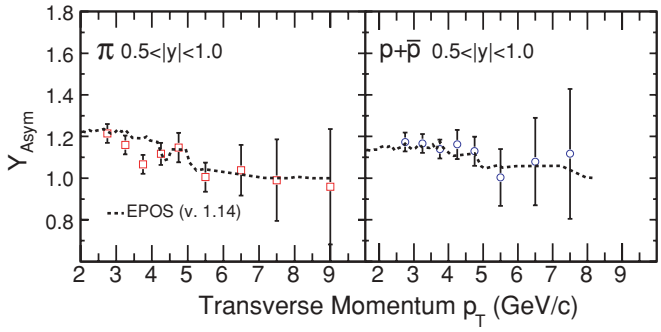

FIG. 8. (Color online) High transverse-momentum rapidity asymmetry factor ($Y_{\rm Asym}$) for $\pi^+ + \pi^-$ and $p + \bar{p}$ for $0.5 < |y| < 1.0$ for minimum bias d+Au collisions at $\sqrt{s_{NN}} = 200$ GeV compared to the EPOS model [7]. See text for more details.

B. Comparison to the multiple scattering+shadowing+energy loss model

Next we compare the high $p_{\rm T}$ charged pion $Y_{\rm Asym}$ to a model that includes only coherent multiple scattering, which leads to transverse-momentum broadening (Cronin effect) and to calculations with the addition of power corrections (dynamical shadowing) and energy loss in cold nuclear matter [3]. In this model a systematic calculation of the coherent multiple parton scattering in p+A collisions is carried out in terms of the perturbative QCD factorization approach. It also incorporates initial state parton energy loss in the perturbative calculations.

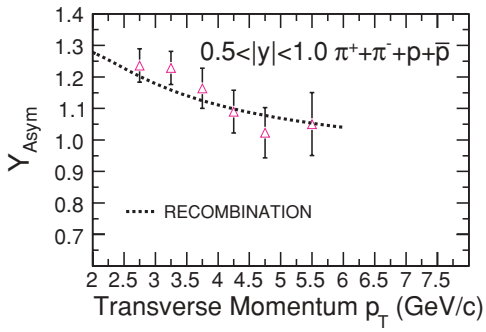

FIG. 9. (Color online) High transverse-momentum rapidity asymmetry factor ($Y_{\rm Asym}$) for $\pi^+ + \pi^- + p + \bar{p}$ and $0.5 < |y| < 1.0$ in 0–20% central d+Au collisions at $\sqrt{s_{NN}} = 200$ GeV compared to the recombination model [6]. See text for more details.

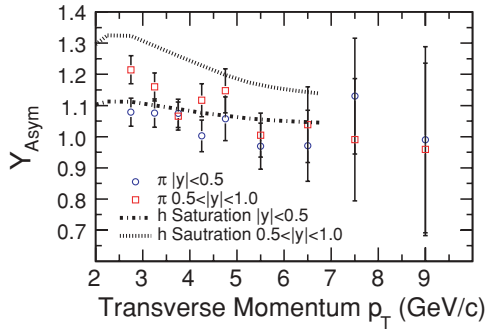

FIG. 10. (Color online) High transverse-momentum rapidity asymmetry factor ($Y_{\rm Asym}$) for $\pi^+ + \pi^-$ at $|y| < 0.5$ and $0.5 < |y| < 1.0$ for minimum bias d+Au collisions at $\sqrt{s_{NN}} = 200$ GeV compared to the saturation model [4]. See text for more details.

We observe (Fig. 7) that in both rapidity regions model expectations from the Cronin effect, for $2.5 < p_T < 5\,\mathrm{GeV}/c$, are in qualitative disagreement with the data. This indicates that multiple scattering is not the source of the observed asymmetry. Figure 7 shows also a comparison of the charged pion data with results of calculations that incorporate multiple scattering, dynamical shadowing, and a varying degree of energy loss in cold nuclear matter. The calculation, labeled as Vitev-I, has a slightly larger effective energy loss in cold nuclear matter than the one labeled Vitev-II. For $|y| < 0.5$, both the Vitev-I and Vitev-II results are in reasonable agreement with the data within errors. For $0.5 < |y| < 1.0$, the Vitev-I result slightly overpredicts the measured $Y_{\rm Asym}$. The model calculations beyond $p_{\rm T} > 3\,\mathrm{GeV}/c$ are independent of $p_{\rm T}$, whereas the measured $Y_{\rm Asym}$ tends to decrease with $p_{\rm T}$.

For the Vitev models the rapidity dependence of $Y_{\rm Asym}$ seems to be sensitive to effective energy loss. The decrease in $Y_{\rm Asym}$ with p_T in the model is restricted to $p_T < 2.5\,\mathrm{GeV}/c$. It will be important to have predictions from this model for proton and antiprotons to investigate the possible particle species dependence of multiple scattering in d+Au collisions.

C. Comparison to the EPOS model

In Fig. 8 the measured $Y_{\rm Asym}$ for $\pi^+ + \pi^-$ and $p + \bar{p}$ for $0.5 < |y| < 1.0$ are compared to the results from the EPOS model. In the EPOS model [7] elastic and inelastic parton ladder splitting are the key processes. A parton ladder refers to the dynamical process of parton–parton scattering with successive emission of partons. The emission process can be an initial-state, spacelike cascade or final-state, timelike cascade. The elastic splitting in this model can be related to screening and saturation, whereas inelastic splitting is related to the hadronization process. This phenomenological model has been very successful in describing the inclusive charged hadron d+Au data [7].

The EPOS model predictions (v. 1.14) are consistent with the measured $Y_{\rm Asym}$ values for both charged pions and $p + \bar{p}$.

D. Comparison to the recombination model

The recombination model reproduces some of the observed features of RHIC data [6,26]. It successfully describes the Cronin effect for d+Au data without any need for k_T broadening in initial-state interactions. There were questions raised concerning issues such as decrease in entropy of the system and the spatial extent of the recombining subsystems. These are addressed in the Refs. [6,26]. So it is useful to compare the experimental measurements with this model to investigate the relative importance of various physical processes.

Figure 9 compares model predictions with the measured $Y_{\rm Asym}$ for $\pi^+ + \pi^- + p + \bar{p}$ for the rapidity region $0.5 < |y| < 1.0$ in 0–20% central d+Au collisions. The model predictions from Ref. [6] are consistent with the data. Because the pions are the dominant hadrons produced in d+Au collisions, the $Y_{\rm Asym}$ for $\pi^+ + \pi^- + p + \bar{p}$ is dominated by them. In the absence of predictions from this model for identified hadrons in d+Au data, it is not clear if it can describe the $Y_{\rm Asym}$ for $p + \bar{p}$. One of the reasons for the success of the recombination model in the intermediate p_T range is that in this model a baryon is formed by recombination of three shower and thermal partons, whereas a meson needs only two, resulting in a higher yield at larger momentum for baryons [6]. A comparison of model calculations separately for charged pions and $p + \bar{p}$ is important to test the recombination mechanism in d+Au collisions. The observed weak species dependence and almost similar $p_{\rm T}$ dependence of $Y_{\rm Asym}$ can be a crucial test for such model calculations.

E. Comparison to the saturation model

Finally, we compare our charged pion measurements to calculations from saturation models [4]. In such models the particle production is determined by the high gluon density in the Au nucleus and the deuteron. The model had successfully described the suppression of high p_T hadron yields at forward rapidities for d+Au data relative to $p + p$ data at RHIC. In contrast to a naive multiple-scattering picture, where one expects enhancement due to the Cronin effect to be more significant for larger forward rapidities due to the increase in the number of scattering centers while probing smaller values of x, the saturation models give a completely opposite result [33]. For this model the momentum range where $Y_{\rm Asym} > 1$ is determined by the saturation and geometrical scales in the model, as well as the onset of the gluon saturation.

In Fig. 10 we compare the $Y_{\rm Asym}$ data for charged pions with the $Y_{\rm Asym}$ predictions for inclusive hadrons. Such a comparison is reasonable as $\pi^+ + \pi^-$ are the dominant hadrons produced in d+Au collisions. Further, the $Y_{\rm Asym}$ values for $\pi^+ + \pi^-$ are similar to those for $p + \bar{p}$. The model calculations presented are carried out with a nonperturbative scale of 1 GeV to account for additional momentum broadening associated with hadronic rescattering processes [4]. The model calculations are in reasonable agreement for $|y| < 0.5$ and give the correct decreasing trend for $Y_{\rm Asym}$ vs. p_T. The prediction of a strong centrality dependence at midrapidity is not observed [5]. Such models are expected to work better at forward rapidities at

RHIC. The models give larger asymmetries than data for $0.5 < |y| < 1.0$.

In this section we compared the $Y_{\rm Asym}$ vs. p_T to various model calculations. The $Y_{\rm Asym}$ vs. p_T dependence rules out models based on incoherent initial multiple partonic scattering and independent fragmentation. The models based only on nuclear shadowing cannot account for the measured $Y_{\rm Asym}$. Models incorporating multiple scattering, dynamical shadowing, and energy loss in cold nuclear matter are in reasonable agreement with the data for $|Y| < 0.5$. However, the $Y_{\rm Asym}$ being independent of p_T ($>3\,{\rm GeV}/c$) is inconsistent with the measurements at higher rapidity. Qualitatively, features of decrease in $Y_{\rm Asym}$ with p_T are in agreement with CGC-type models. However, there is a lack of quantitative agreement at higher rapidities where this model is expected to work better. The EPOS and recombination models are in best quantitative agreement with the data. The actual test of the recombination model is only possible when the calculations are available for $Y_{\rm Asym}$ for identified baryons and mesons.

V. NUCLEAR MODIFICATION FACTOR

The gluon saturation effects are believed to manifest themselves in terms of suppression of transverse distributions below the saturation scale. The onset of gluon saturation and the saturation scale, in turn, depend on the gluon density and the rapidity of the measured particles. The saturation scale at RHIC is expected to be $\sim 2\,{\rm GeV}^2$ and depends on the colliding nuclei and rapidity as $\sim A^{1/3}e^{\lambda y}$ [4,33,34]. The value of λ lies between 0.2–0.3 and is obtained from fits to HERA data [35]. It is important to study the variation of the nuclear modification factor ($R_{\rm CP}$) as a function of rapidity. The $R_{\rm CP}(y)$ and the $Y_{\rm Asym}(p_T)$ together can provide a more stringent constraint on particle production models. Although the present data do not have large rapidity span, we will explore the variation of $R_{\rm CP}$ for identified hadrons from forward to backward rapidity. $R_{\rm CP}$ is defined as

$$R_{\rm CP} = \frac{(d^2N/dp_T dy/\langle N_{\rm bin}\rangle)|_{\rm central}}{(d^2N/dp_T dy/\langle N_{\rm bin}\rangle)|_{\rm periph}}, \qquad (1)$$

where $d^2N/dp_T dy$ is the differential yield per event in d+Au collisions for a given centrality class.

Figure 11 shows the p_T integrated $R_{\rm CP}$ for $\pi^+ + \pi^-$ and $p + \bar{p}$ with rapidity $|y| < 1.0$ and $p_T > 2.5\,{\rm GeV}/c$. There may be a decrease in $R_{\rm CP}$ for $\pi^+ + \pi^-$ from backward rapidity (gold-side) to forward rapidity (deuteron side). Within the systematic errors (shown as boxes) the $R_{\rm CP}$ for proton+antiproton is almost constant within the rapidity range studied. Also shown for comparison are the $R_{\rm CP}$ values for inclusive charged hadrons as a function of pseudorapidity [5]. The dependences are slightly weaker than observed by BRAHMS for inclusive charged hadrons in the forward rapidity region [36].

VI. PARTICLE RATIOS

Figure 12 shows the π^-/π^+ and $\bar{p}/p$ ratios for $2.5 < p_T < 10\,{\rm GeV}/c$ as functions of rapidity for peripheral (40–100%)

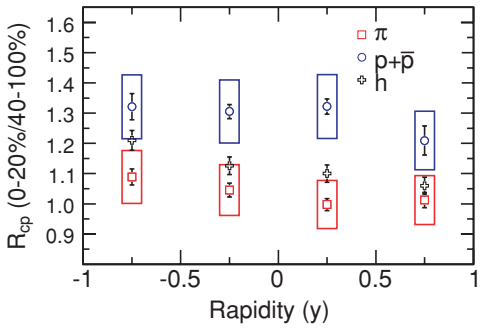

FIG. 11. (Color online) Variation of nuclear modification factor ($R_{\rm CP}$) for $\pi^+ + \pi^-$ and $p + \bar{p}$ with rapidity for $p_T > 2.5\,{\rm GeV}/c$ for d+Au collisions at $\sqrt{s_{NN}} = 200$ GeV. Also shown for comparison are the $R_{\rm CP}$ values for inclusive charged hadrons as a function of pseudorapidity [5]. The errors shown as boxes are the systematic errors. The error due to number of binary collisions is ~14% and is not shown in the figure.

and n-tag events for d+Au collisions at $\sqrt{s_{NN}} = 200\,{\rm GeV}$. The π^-/π^+ ratio is unity for both n-tag and peripheral events in the negative (gold-side) rapidity region. For the positive-region, the absolute value of π^-/π^+ ratio is smaller for n-tag events compared to peripheral d+Au data; however considering the systematic errors (boxes), they are also consistent with unity. The systematic errors do not allow for any strong conclusions regarding the differences, which are expected from the valence quark and isospin effects at high p_T for n-tag events. The $\bar{p}/p$ ratios are similar within the systematic errors for the two event classes. The $\bar{p}/p$ ratios are slightly smaller than observed for $p + p$ data.

To cancel out most of the systematic errors (listed in Table III), we have plotted the double ratio of $(\pi^-/\pi^+)_{n-{\rm tag}}/(\pi^-/\pi^+)_{40-100\%}$ and $(\bar{p}/p_{n-{\rm tag}}/(\bar{p}/p)_{40-100\%}$ in Fig. 13. The double ratio clearly shows the difference between the π^-/π^+ ratio in the forward and backward rapidity regions when we compare peripheral d+Au collisions and n-tag events. A small difference for $\bar{p}/p$ ratios between n-tag and peripheral d+Au collisions is observed for both rapidities. The boxes shown in the Fig. 13 are systematic errors on the double ratio, which were calculated by varying the distance of closest approach of the tracks from the vertex (error of ~1%), dE/dx cuts (error of ~1%), p_T cuts (error of ~ 2%), and small change in rapidity range (error of ~3%). The total systematic error on the double ratio is ~4%.

Because the neutron-tagged collisions and 40–100% d+Au collisions are different mostly in the valence quark content (isospin) in the projectile (p+Au vs. d+Au), the particle ratios and the double ratios can be used to get an idea of relative fragmentation of d and u quarks to protons, as well as u quarks to π^+ and π^-. The details of the procedure relating the measured ratios to the fragmentation ratios are given in Ref. [9]. The x_q^π value for charged pions from NLO pQCD calculations using the Albino-Kniehl-Kramer (AKK) set of fragmentation functions (FFs) [37] is between 10 and 20% [38] for the measured p_T range in this work. x_q^π is the fractional contribution from quarks to pion production relative to the total (from both quarks and gluons) pion production. This range in x_q^π value from the NLO pQCD calculations are

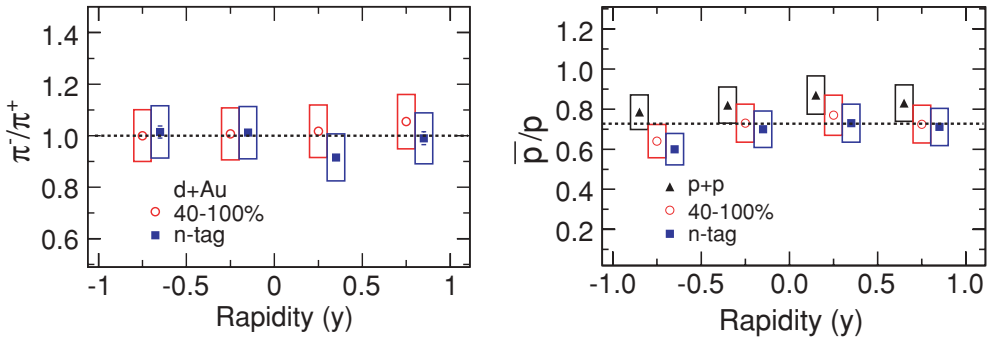

FIG. 12. (Color online) Variation of π^-/π^+ and $\bar{p}/p$ with rapidity for $2.5 < p_T < 10\,\mathrm{GeV}/c$ for peripheral (40–100%) and n-tag events for d+Au collisions at $\sqrt{s_{NN}} = 200$ GeV. Also shown for comparison are the $\bar{p}/p$ for minimum bias $p + p$ collisions. The boxes are the systematic errors. The ratios for n-tag events are shifted by 0.05 units in rapidity and those for $p + p$ collisions by -0.05 units in rapidity for clarity of presentation.

obtained by varying the factorization scales from $0.5\,p_T$ to $2\,p_T$. The NLO pQCD calculations with AKK FFs agree reasonably well with charged pion measurements at RHIC [21]. It has also been shown that $D_u^{\pi^+} < 1$ and $D_u^{\pi^-} > 0$, where D_u^{π} is the u-quark fragmentation to pion in the p_T region studied [9]. Our results of π^-/π^+ double ratio at forward rapidity are qualitatively consistent with x_q^{π} from AKK and $D_u^{\pi^+}$ [9]. Further detailed calculations and experimental data with high statistics are needed to extend this study to higher p_T and extract parameters related to quark and gluon contribution to the hadron production (x_q^{π}) and fragmentation function D_u^{π}.

VII. SUMMARY

We have presented transverse-momentum spectra for identified charged pions, protons, and antiprotons from d+Au collisions in various centrality classes at $\sqrt{s_{NN}} = 200$ GeV. The transverse-momentum spectra are measured in four rapidity bins for $-1 < y < 1$ over the range $2.5 < p_T < 10\,\mathrm{GeV}/c$. The rapidity, p_T, centrality, and species dependence of the rapidity asymmetry Y_{Asym} has been studied. We have also presented the rapidity dependence of the nuclear modification factor and the π^-/π^+ and $\bar{p}/p$ ratios for the rapidity range $|y| < 1.0$ and $p_T > 2.5\,\mathrm{GeV}/c$.

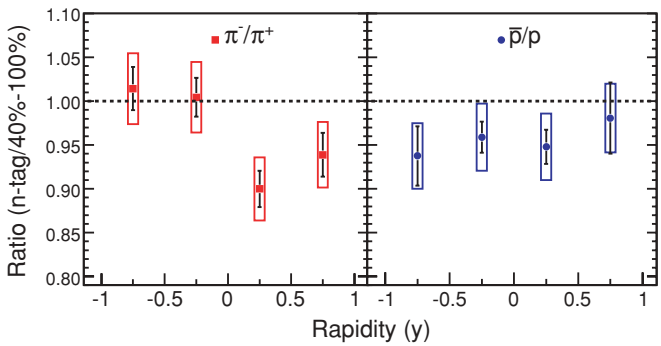

FIG. 13. (Color online) Variation of double ratio $(\pi^-/\pi^+)_{n-\mathrm{tag}}/(\pi^-/\pi^+)_{40--100\%}$ and $(\bar{p}/p)_{n-\mathrm{tag}}/(\bar{p}/p)_{40\text{-}100\%}$ with rapidity for $2.5 < p_T < 10\,\mathrm{GeV}/c$ for d+Au collisions at $\sqrt{s_{NN}} = 200$ GeV. The boxes are the systematic errors.

The Y_{Asym} is found to be larger for $0.5 < |y| < 1.0$ than for $|y| < 0.5$ in the range $2.5 < p_T < 5.0\,\mathrm{GeV}/c$. For higher p_T the Y_{Asym} approach 1 for both charged pions and $p + \bar{p}$. From these observations we conclude that possible sources of nuclear effects in d+Au collisions, such as parton saturation, nuclear shadowing, or energy loss in cold nuclear matter, have a strong rapidity dependence that vanishes for $p_T (> 5.5\,\mathrm{GeV}/c$. The observed Y_{Asym} vs. p_T dependence rules out models based on incoherent initial multiple partonic scattering and independent fragmentation.

Comparison to models based on nuclear shadowing reveals that incorporation of extremes of gluon shadowing at low x does not reproduce the measured Y_{Asym}. This provides an upper limit on the contribution of nuclear shadowing to the Y_{Asym}. Models incorporating multiple scattering, dynamical shadowing, and energy loss in cold nuclear matter are in reasonable agreement with the data for $|y| < 0.5$. However, the Y_{Asym} being independent of p_T ($> 3\,\mathrm{GeV}/c$) is inconsistent with the measurements at higher rapidity. Qualitatively, features of decrease in Y_{Asym} with p_T and R_{CP} with y are in agreement with CGC-type models. However, there is a lack of quantitative agreement at higher rapidities where this model is expected to work better. Further, the absence of very strong centrality dependence at midrapidity in the data is in contrast to the predictions from CGC models.

The EPOS and recombination models are in best quantitative agreement with the data. The actual test of the recombination model is only possible when the calculations are available for Y_{Asym} for identified baryons and mesons. It will be interesting to see if this model can explain the observed weak species dependence and similar p_T dependence of Y_{Asym} for $\pi^+ + \pi^-$ and $p + \bar{p}$.

In general, the study of identified hadron Y_{Asym} as a function of many variables (y, p_T, centrality and particle type) for d+Au collisions has been able to provide some definitive insight on mechanisms of particle production in d+Au collisions at $\sqrt{s_{NN}} = 200$ GeV. The $Y_{\mathrm{Asym}}(p_T)$ together with $R_{\mathrm{CP}}(y)$ can provide a more stringent constraint on particle production models. It may be mentioned that a detailed of study of particle yields ($p_T < 3\,\mathrm{GeV}/c$) at midrapidity and forward rapidity in STAR has revealed a possible alternative explanation of the pseudorapidity dependence of R_{CP} from a

purely geometrical picture. The decrease in R_{CP} from negative (backward) to positive (forward) rapidity can be explained by considering the initial asymmetry in particle production in d+Au collisions compared to the symmetric $p + p$ collisions [39].

The ratios π^-/π^+ and $\bar{p}/p$ have been studied for peripheral and n-tag events for d+Au collisions to see the possible valence quark effect. For the range $2.5 < p_T < 10\,\mathrm{GeV}/c$ and the rapidity region on the deuteron-side, the ratios for n-tag events are smaller than for peripheral events. However, within the systematic errors it is difficult to make strong conclusions of valence quark effects on particle production at high p_T. The $\bar{p}/p$ ratios are observed to be systematically lower than corresponding values from $p + p$ collisions.

The double ratio between n-tag events and 40–100% peripheral collision events does reveal a clear enhancement in π^+ production relative to π^- at forward rapidity (deuteron side). No such enhancement is observed at the backward rapidity (gold side). This is qualitatively consistent with isospin effect using constraint from EMC measurements on $D_u^{\pi^-}/D_u^{\pi^+}$, and $x_q^\pi = 10$–20% given by the NLO pQCD calculations. A future, high statistics run for d+Au collisions at RHIC may be able to provide data that will lead to a still better insight into valence quark and gluon contribution, as well as isospin effects at high p_T.

ACKNOWLEDGMENTS

We thank S. Albino, R. Hwa, I. Vitev, R. Vogt, K. Werner, and C. B. Yang for providing us the results for the different model calculations and many useful discussions. We thank the RHIC Operations Group and RCF at BNL, and the NERSC Center at LBNL for their support. This work was supported in part by the Offices of NP and HEP within the U.S. DOE Office of Science; the U.S. NSF; the BMBF of Germany; CNRS/IN2P3, RA, RPL, and EMN of France; EPSRC of the United Kingdom; FAPESP of Brazil; the Russian Ministry of Science and Technology; the Ministry of Education and the NNSFC of China; IRP and GA of the Czech Republic; FOM of the Netherlands; DAE, DST, and CSIR of the Government of India; Swiss NSF; the Polish State Committee for Scientific Research; SRDA of Slovakia; and the Korea Science & Engineering Foundation.

[1] R. Vogt, Phys. Rev. C **70**, 064902 (2004); and private communication.
[2] D. Antreasyan, J. W. Cronin, H. J. Frisch, M. J. Shochet, L. Kluberg, P. A. Piroue, and R. L. Sumner, Phys. Rev. D **19**, 764 (1979).
[3] J. Qiu and I. Vitev, Phys. Lett. **B632**, 507 (2006); I. Vitev, *ibid.* **B562**, 36 (2003).
[4] D. Kharzeev, Y. Kovchegov, and K. Tuchin, Phys. Lett. **B599**, 23 (2004); K. Tuchin (private communication).
[5] STAR Collaboration, J. Adams *et al.*, Phys. Rev. C **70**, 064907 (2004).
[6] R. C. Hwa, C. B. Yang, and R. J. Fries, Phys. Rev. C **71**, 024902 (2005).
[7] K. Werner, F. Liu, and T. Pierog, Phys. Rev. C **74**, 044902 (2006).
[8] STAR Collaboration, J. Adams *et al.*, Phys. Rev. Lett. **92**, 052302 (2004).
[9] European Muon Collaboration, J. J. Aubert *et al.*, Phys. Lett. **B160**, 417 (1985); M. Arneodo *et al.*, Nucl. Phys. **B321**, 541 (1989).
[10] OPAL Collaboration, G. Abbiendi *et al.*, Eur. Phys. J. C **16**, 407 (2000).
[11] K. H. Ackerman *et al.*, Nucl. Instrum. Methods A **499**, 624 (2003).
[12] M. Anderson *et al.*, Nucl. Instrum. Methods A **499**, 659 (2003).
[13] C. Adler *et al.*, Nucl. Instrum. Methods A **499**, 433 (2003); **461**, 337 (2001).
[14] K. H. Ackermann *et al.*, Nucl. Instrum. Methods A **499**, 713 (2003).
[15] STAR Collaboration, J. Adams *et al.*, Phys. Rev. Lett. **91**, 072304 (2003).
[16] STAR Collaboration, C. Adler *et al.*, Phys. Rev. Lett. **89**, 202301 (2002); B. Choi, Ph.D. dissertation, University of Texas (2003).
[17] D. Kharzeev, E. Levin, and M. Nardi, Nucl. Phys. **A730**, 448 (2004); L. Hulthén and M. Sagawara, *Handbuch der Physik* (Springer-Verlag, Berlin, 1957), Vol. 39.
[18] R. E. Ansorge *et al.*, Z. Phys. C **43**, 357 (1989).
[19] X. N. Wang and M. Gyulassy, Phys. Rev. D **44**, 3501 (1991). Version 1.382 is used.
[20] M. Shao *et al.*, Nucl. Instrum. Methods A **558**, 419 (2006).
[21] STAR Collaboration, J. Adams *et al.*, Phys. Lett. **B637**, 161 (2006).
[22] H. Bichsel, Nucl. Instrum. Methods A **562**, 154 (2006); H. Bichsel, D. E. Groom, and S. R. Klein, Phys. Lett. **B592**, 242 (2004); Proceedings of 8th International Conference on Advance Technology and Particle Physics, ICATPP 2003, p. 448.
[23] STAR Collaboration, J. Adams *et al.*, Phys. Lett. **B616**, 8 (2005).
[24] STAR Collaboration, C. Adler *et al.*, Phys. Rev. Lett. **86**, 4778 (2001).
[25] X.-N. Wang, Phys. Lett. **B565**, 116 (2003).
[26] V. Greco, C. M. Ko, and P. Levai, Phys. Rev. Lett. **90**, 202302 (2003); Phys. Rev. C **68**, 034904 (2003); R. J. Fries, B. Muller, C. Nonaka, and S. A. Bass, Phys. Rev. Lett. **90**, 202303 (2003); Phys. Rev. C **68**, 044902 (2003).
[27] PHOBOS Collaboration, B. B. Back *et al.*, Phys. Rev. C **70**, 061901(R) (2004); Phys. Rev. Lett. **93**, 082301 (2004).
[28] BRAHMS Collaboration, I. Arsene *et al.*, Phys. Rev. Lett. **94**, 032301 (2005).
[29] K. J. Eskola, V. J. Kolhinen, and P. V. Ruuskanen, Nucl. Phys. **B535**, 351 (1998); K. J. Eskola, V. J. Kolhinen, and C. A. Salgado, Eur. Phys. J. C **9**, 61 (1999).
[30] L. Frankfurt, V. Guzey, and M. Strikman, Phys. Rev. D **71**, 054001 (2005).
[31] A. D. Martin, R. G. Roberts, and W. J. Stirling, Phys. Lett. **B354**, 155 (1995).
[32] B. A. Kniehl, G. Kramer, and B. Potter, Nucl. Phys. **B597**, 337 (2001).
[33] D. Kharzeev, Y. V. Kovchegov, and K. Tuchin, Phys. Rev. D **68**, 094013 (2003).

[34] L. McLerran and R. Venugopalan, Phys. Rev. D **49**, 2233 (1994); **59**, 094002 (1999); E. Iancu, A. Leoidov, and L. D. McLerran, Nucl. Phys. **A692**, 583 (2001); A. Dumitru and J. Jalilian-Marian, Phys. Lett. **B547**, 15 (2002); F. Gelis and J. Jalilian-Marian, Phys. Rev. D **66**, 014021 (2002).
[35] ZEUS Collaboration, J. Breitweg *et al*., Phys. Lett. **B407**, 432 (1997).
[36] BRAHMS Collaboration, I. Arsene *et al*., Phys. Rev. Lett. **93**, 242303 (2004).
[37] S. Albino, B. A. Kniehl, and G. Kramer, Nucl. Phys. **B725**, 181 (2005).
[38] B. Mohanty (for the STAR Collaboration), arXiv:0705.0953.
[39] J. Putschke (for the STAR Collaboration), J. Phys. Conf. Ser. **5**, 37 (2005); STAR Collaboration, B. I. Abelev *et al*., arXiv:nucl-ex/0703016.